Heat Transfer in a Two-Dimensional Crystalline Complex (Dusty) Plasma

S. Nunomura,* D. Samsonov, S. Zhdanov, and G. Morfill
CIPS, Max-Planck-Institut für Extraterrestrische Physik, D-85740 Garching, Germany
(Received 15 July 2004; published 7 July 2005)

Heating and heat transfer were studied in a two-dimensional crystalline complex plasma at the kinetic level. The lattice was formed of microspheres levitated in a plasma sheath. One half of the crystal was heated anisotropically to obtain higher kinetic temperatures in one direction and heat conduction was observed in real time. It was found that the longitudinal phonons conduct heat better than the transverse. The thermometric conductivity coefficient was measured to be 53 mm^2/s for longitudinal heating and 30 mm^2/s for transverse heating. Heat decay lengths and energy exchange times between the temperature components were determined.

DOI: 10.1103/PhysRevLett.95.025003 PACS numbers: 52.27.Lw, 52.35.Fp

There are three basic mechanisms of heat transfer: radiation, convection, and conduction. While the first two are significant in gases and liquids, the last is predominant in solids [1]. Two energy carriers conduct heat in solids: electrons in metals and phonons in insulators and semiconductors. Although most practical aspects of heat conduction in ordinary materials have moved into the category of engineering problems [1], there are some topics, such as phonon thermal conductivity [2] in semiconductor superlattices, which have attracted attention recently because of the applications in thermoelectronic and optoelectronic devices.

The microscopic dynamical origin of heat transfer is a long-standing fundamental problem in statistical mechanics [3] with the derivation of Fourier's law from a statistical-mechanics calculation as the ultimate goal. Theoretical and simulation efforts have concentrated on regular and irregular one-dimensional chains of linear and nonlinear oscillators [4–6]; however, only a few attempts were made to simulate two-dimensional lattices (see the review in [3]). Until a few years ago, it seemed that research into heat conduction by means of lattice dynamics could only be conducted theoretically or using simulations, since it is very difficult to observe the motion of atoms and molecules in usual crystals in real time (due to the extremely short time and spatial scales). However, such experimental studies of crystal properties have now become feasible with the recent advent of plausible model systems, for example, colloidal suspensions [7], granular media [8], and complex plasmas [9].

Complex plasmas consist of charged micron-sized particles levitated in a discharge plasma. The grains interact with each other via a Yukawa (screened Coulomb) potential. Complex plasmas can exist in gaseous, liquid, and crystalline phase states [9]. Damping of the particle motion due to collisions with neutrals is weak, compared to colloids, and therefore the waves (phonons) are not overdamped in complex plasmas. Complex plasmas were used as model systems to study Mach cones [10], solitons [11], waves [12,13], and shocks [14] at the kinetic level (i.e., motion of every particle).

In this Letter we investigate the heat transfer in a crystalline complex plasma experimentally at the kinetic level. Analogously to solids, the heat in plasma crystals is conducted by phonons. Unlike in solids, the phonons are affected by the friction of the neutral gas making the heat transfer more complicated.

We performed the experiment in a capacitively coupled radio-frequency (13.56 MHz) discharge. A schematic view of the experimental setup (similar to that of Ref. [13]) is shown in Fig. 1. An argon plasma was generated by applying the power of 4 W between the lower electrode and the vacuum vessel. The gas pressure was maintained at 0.8 Pa by regulating the gas flow at 1.5 sccm. This low pressure was chosen to reduce the damping of particle motion by the gas drag and thus to slow down their cooling.

A particle monolayer was prepared by introducing plastic microspheres into the plasma. These particles were

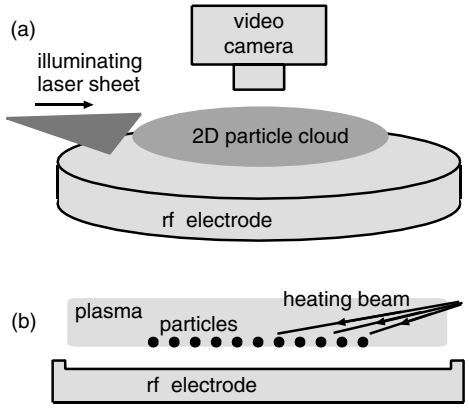

FIG. 1. Sketch of apparatus. (a) Oblique view. The particles are illuminated with a horizontal sheet of a doubled Nd:YAG laser (532 nm) and viewed from the top using a video camera. The heating of the particle cloud was provided by light pressure of an argon-ion laser beam scanned randomly. (b) Side view. The rf voltage is applied between the electrode and the grounded chamber creating a plasma. Spherical particles charge negatively and form a monolayer levitating in the plasma sheath above the lower electrode.

charged negatively and suspended by the electric field in the plasma sheath above the lower electrode. Because of the repulsive Coulomb interaction among the particles, they formed a monolayer triangular (hexagonal) lattice. The lattice had a few percent of defects (five and sevenfold cells). The suspension was composed of approximately 9000 particles and its diameter was ≈ 8 cm (particle separation $a = 0.81$ mm). The monodisperse microspheres had a diameter of 8.9 ± 0.1 μm and a mass of 5.57×10^{-13} kg. Analyzing the phonon spectra [12] we estimated that the particle charge $Q = 14600e$ and the lattice parameter $\kappa = a/\lambda_D \approx 1.0$, where λ_D is the screening length.

To observe the random motion of the particles, we illuminated the monolayer with a horizontal thin laser sheet. The central part of the particle cloud was viewed from the top with a digital video camera, which had a field of view of 23.5×23.5 mm and included ≈ 900 particles. The images were recorded for 23.3 seconds at 22 frames per second. Analyzing the images, we identified the particle positions and traced them from one frame to the next. Particle velocities v_x and v_y were calculated from their displacements in two consecutive frames.

We "heated" the particles (increased their kinetic temperature, or in other words, their kinetic energy of random motion) using the light pressure of a laser beam whose intensity was modulated by a white noise with frequency up to 500 Hz. The beam was randomly moved over one half of the monolayer using a pair of galvanometer mirrors operated by white noise with cutoff frequency 200 Hz. The beam was focused on the monolayer and made an angle of $\approx 10°$ to the horizontal plane. The beam spot (with full width at half maximum of 1.5 mm in x and 0.26 mm in y directions) illuminated only a single particle at a time. This particle was then pushed in the direction of the beam. The coordinate x is defined parallel to the laser beam and y perpendicular to it. The main crystal axis of the lattice was aligned with y ($\mathbf{a} \parallel y$).

With this technique we can heat the lattice anisotropically; i.e., the resulting kinetic temperature is higher in the x direction than in y. By confining this heating to one half of the plasma crystal, we can use it to study how heat is transferred by longitudinal and transverse waves. Since the longitudinal waves are faster than the transverse waves [15], the thermometric conductivity [16] ($\chi = \kappa/\rho c_p$, where κ is the thermal conductivity, ρ is the density, and c_p is the specific heat at constant pressure) should be different if heat is transferred by different waves. The experimental procedure is then to heat one half of the crystal with the beam (and hence the particle perturbation) parallel to the hot-cold interface, and in a second experiment perpendicular to the interface. If the hot-cold interface is perpendicular to the laser beam [Fig. 2(a)], we expect the heat to be transferred in the direction of the particle excited motion and therefore mostly by longitudinal phonons. In the case, when the hot-cold interface is parallel to the beam [Fig. 2(d)], the heat should be transferred in the direction perpendicular to the excited motion and thus mostly by transverse phonons.

Figure 2 shows the temperature profiles across the crystal at three different laser powers $P = 1$, 2, and 4 W. The temperature profiles look similar for all cases of heat propagation [Fig. 2(b), 2(c), 2(e), and 2(f)]. The temperature saturated at the left (heated) side of the lattice and exponentially decreased to the initial value at the right (cold) edge. The temperature increased with laser power up to 0.6 eV at $P = 4$ W. The corresponding amplitude of

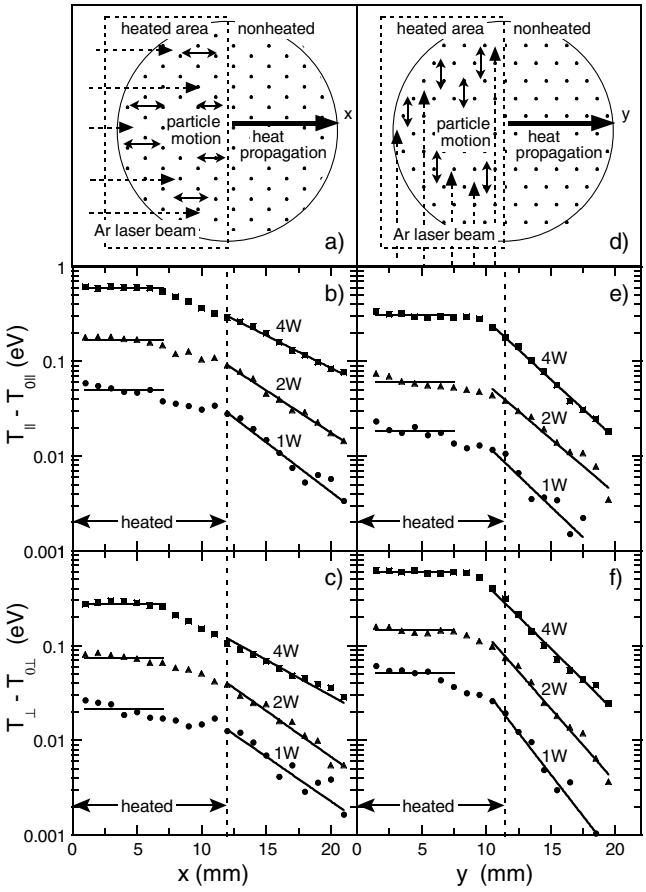

FIG. 2. Kinetic temperature distribution in a monolayer plasma crystal. The left side of the lattice was heated by light pressure of a randomly scanned laser beam. (a) Sketch of the longitudinally heated area. The heating beam is directed perpendicular to the hot-cold interface (dotted line) and parallel to the direction of the heat propagation. (b) Kinetic energy component parallel to the direction of heat propagation. (c) Kinetic energy component perpendicular to the direction of heat propagation. (d) Sketch of the transverse heated area. The heating beam is directed parallel to the hot-cold interface (dotted line) and perpendicular to the direction of the heat propagation. (e) Kinetic energy component parallel to the direction of heat propagation. (f) Kinetic energy component perpendicular to the direction of heat propagation. We subtracted the equilibrium kinetic energy without the lattice heating. This shows that the kinetic energy decays exponentially outside of the heated area (solid lines).

particle random motion was $0.07a$. We confirmed that the initial temperature (without heating $P = 0$) was homogeneous and isotropic over the whole monolayer $T_{0\parallel} = T_{0\perp} = 0.04$ eV. This value was subtracted in all plots [Fig. 2(b), 2(c), 2(e), and 2(f)] to emphasize the exponential decay of the temperature in the nonheated part of the lattice. Deep inside the heated area, the parallel and perpendicular kinetic temperatures are not equal to each other because the heating is anisotropic. Their ratio is approximately 2.5 and it was limited by the energy exchange between the temperature components.

Heat transport in our experiment is described by the equations:

$$\partial T_\parallel/\partial t + \nabla \cdot \mathbf{q}_\parallel = (T_\perp - T_\parallel)/\tau - 2\nu T_\parallel + S_n + S_l \quad (1)$$

$$\partial T_\perp/\partial t + \nabla \cdot \mathbf{q}_\perp = (T_\parallel - T_\perp)/\tau - 2\nu T_\perp + S_n, \quad (2)$$

where indices $\parallel, \perp$ indicate the direction parallel or perpendicular to the direction of heat propagation, $T_{\parallel,\perp}$ are the kinetic temperatures, S_n is the natural heat source, S_l is the heat source due to laser heating, ν is the Epstein damping rate, and τ is the energy exchange time between $T_\parallel$ and $T_\perp$. We assume that the normalized thermal flux $\mathbf{q}_{\parallel,\perp} = -\chi_{\parallel,\perp}\nabla T_{\parallel,\perp}$ is determined by Fourier's law, χ is the thermometric conductivity coefficient (isotropic in the first approximation), which is different in the case of parallel (longitudinal) [Fig. 2(a)–2(c)] and perpendicular (transverse) [Fig. 2(d)–2(f)] heating.

Far outside of the heated area the temperature is $T_\parallel = T_\perp = T_0$, $\partial T_{\parallel,\perp}/\partial t = 0$, and $\mathbf{q} = 0$. Substituting this into Eqs. (1) and (2), we obtain $S_n = 2\nu T_0$. Deep inside the heated area the temperatures are constant $T_\parallel^\infty \neq T_\perp^\infty$, and there are no fluxes; therefore, $S_l = 2\nu(T_\parallel^\infty + T_\perp^\infty - 2T_0)$. The energy exchange time is then given by $\tau = \frac{1}{2\nu}\frac{T_\parallel^\infty - T_\perp^\infty}{T_\perp^\infty - T_0}$. Figure 3 shows the excess kinetic energy $T_\Sigma - 2T_0 (T_\Sigma = T_\parallel + T_\perp)$ inside the heated area and τ as functions of laser power. For our crystal at $\nu = 1.1\ \mathrm{s}^{-1}$, τ was estimated to be ≈ 0.6 s. We checked that the excess kinetic energy is proportional to the heat source of the laser heating, i.e., $T_\Sigma - 2T_0 \propto S_l (\propto P^2)$.

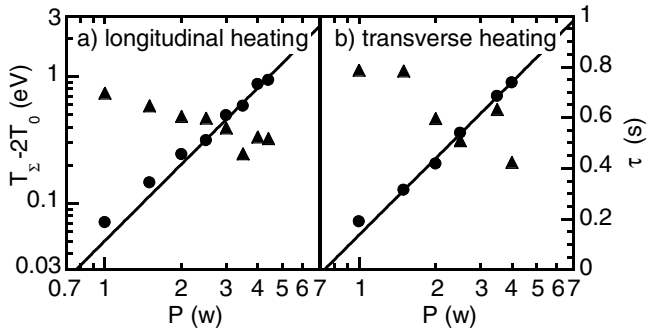

FIG. 3. Excess kinetic energy $T_\Sigma - 2T_0$ (circles) inside the heated area and energy exchange time τ (triangles) vs laser power for longitudinal (a) and transverse (b) heating. A solid line is the least square fit, indicating $T_\Sigma - 2T_0 \propto P^2$.

At the edge of the heated area, where the temperature has a gradient, substituting the fluxes into Eqs. (1) and (2), and assuming that the temperature has two components, isotropic (total) T_Σ and anisotropic $T_\Delta = T_\parallel - T_\perp$ we derive for the steady state:

$$\chi T_\Sigma'' = 2\nu T_\Sigma - 2S_n - S_l(x) \quad (3)$$

$$\chi T_\Delta'' = 2\nu(1 + 1/(\nu\tau))T_\Delta - S_l(x). \quad (4)$$

The thermometric conductivity coefficient is then $\chi = 2\nu L_\Sigma^2$, where L_Σ is the decay length for T_Σ. The decay length for T_Δ is $L_\Delta = L_\Sigma\sqrt{\nu\tau/(1+\nu\tau)}$. The ratio of these decay lengths is $L_\Delta/L_\Sigma \simeq 0.63$ for our experimental conditions. We do not have enough experimental data to measure L_Δ precisely. The total decay length L_Σ is close to the average of $\lambda_\parallel$ and $\lambda_\perp$, the parallel and perpendicular heat decay lengths shown in Fig. 4. Taking $L_\Sigma^l = 4.9 \pm 0.7$ mm for longitudinal heating and $L_\Sigma^{\mathrm{tr}} = 3.7 \pm 0.4$ mm for transverse heating (Fig. 4 for 2 W laser power) we obtain the longitudinal thermometric conductivity coefficient $\chi_l = 53 \pm 14\ \mathrm{mm}^2/\mathrm{s}$ and transverse coefficient $\chi_{\mathrm{tr}} = 30 \pm 6\ \mathrm{mm}^2/\mathrm{s}$.

Figure 4 shows that the heat decay lengths are larger for longitudinal than for transverse heating. This difference indicates that phonons with different speeds (longitudinal and transverse, respectively) are primarily responsible for heat transfer in case of longitudinal and transverse heating. The longitudinal phonons are faster (and therefore have larger decay length) than the transverse ones and should dominate in the case of longitudinal heating.

The heat decay lengths (Fig. 4) for longitudinal heating are significantly shorter than the decay length of the long-wavelength longitudinal phonons λ_{l0} measured in

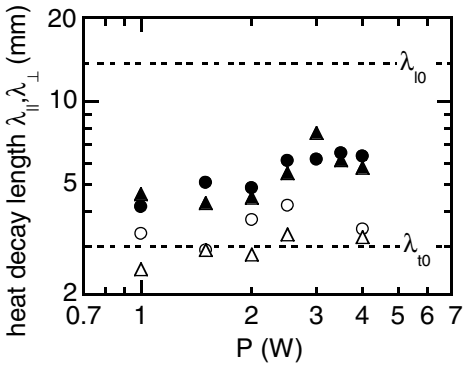

FIG. 4. Parallel (filled circles) and perpendicular (filled triangles) heat decay lengths for longitudinal heating, parallel (open circles) and perpendicular (open triangles) for transverse heating. Dashed lines marked by λ_{l0} and λ_{t0} indicate decay lengths of long-wavelengths compressional and transverse phonons measured in Ref. [15]. The observed heat decay lengths are shorter than those of the long-wavelength longitudinal phonons.

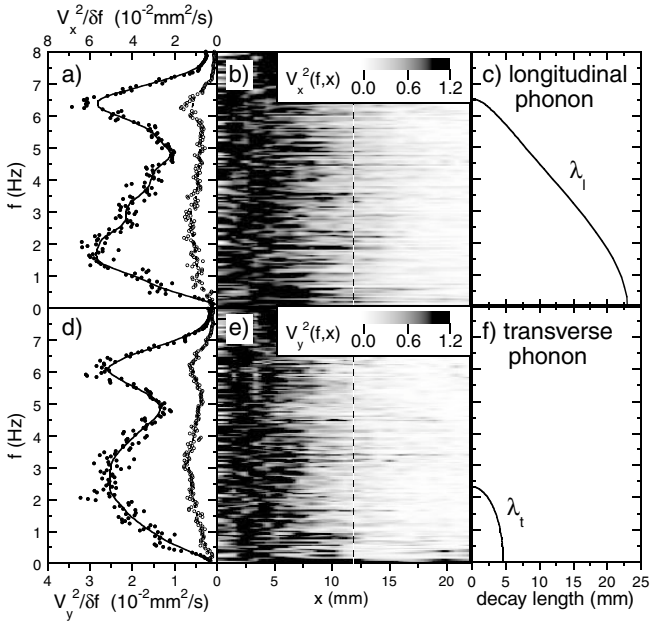

FIG. 5. Spectra of the thermal motion and decay lengths of phonons (longitudinal heating at 4 W). The boundary between the heated and heat propagation regions is located around 12 mm in x, shown by the dashed line. Spectra of (a) longitudinal v_x^2 and (d) transverse v_y^2 motion in the heated region (left curve) and in the heat propagation region (right curve). The energy distribution does not change as the temperature decreases. Spectra of (b) longitudinal v_x^2 and (e) transverse v_y^2 components vs distance and frequency, with the energy distribution without heating subtracted and then normalized by the mean value in the heated area for each frequency. The decay lengths for (c) longitudinal and (f) transverse phonons $\lambda_{l,t}$ differ significantly. The decay length of longitudinal phonons strongly depends on the phonon frequency and significantly exceeds the decay length of transverse phonons. Almost equal observed decay lengths indicate that there is energy exchange between the phonons. The phonons propagate perpendicular to the lattice alignment ($\mathbf{k} \perp \mathbf{a}$).

Ref. [15]. In our opinion, this is due to two reasons: first is that short-wavelength waves (which are slower and therefore have shorter decay length) play a significant role in heat transfer, and second is that some energy is transferred into transverse phonons which are also slower. The parallel and perpendicular heat decay lengths are close to each other in the longitudinal heating experiment because the energy exchange time is shorter than the damping time; i.e., $\tau\nu < 1$. The small value of τ also makes it impossible to obtain a high ratio of the parallel and perpendicular temperature components in our experiment. The increase of the damping lengths with the laser power indicates nonlinear effects.

The transverse heat decay length is close to the decay length of the long-wavelength transverse phonons λ_{t0} (Ref. [15]). It is reduced by the slower short-wavelength transverse waves and increased by the energy exchange with longitudinal phonons. The second mechanism is more efficient because we cannot obtain a high ratio $T_\perp/T_\parallel$ (typical value 2.5). Thus the value obtained for the transverse thermometric conductivity should be considered as the upper limit.

To analyze the distribution of heat phonons in the frequency space, we calculated the spectra of the particle thermal motion for longitudinal heating. Figures 5(a) and 5(d) show the spectra of the longitudinal v_x^2 and transverse v_y^2 motion in the heated (0.5 mm $< x <$ 7.5 mm) and nonheated (15.5 mm $< x <$ 22.5 mm) areas at $P = 4$ W. The spectra have two broad peaks, which correspond to parts of phonon dispersion relation where $d\omega/dk \approx 0$ [12]. The spectra do not change with the distance as the heat propagates and the temperature decreases [Fig. 5(b) and 5(e)], and the heat decay lengths are the same for the longitudinal and transverse phonons. This contradicts the theoretical phonon decay lengths [Fig. 5(c) and 5(f)] calculated from the neutral damping and therefore indicates that there is a redistribution of energy between the frequencies and wave modes. Thus we observe the heat transfer and not just phonon propagation. In other words, we obtained a flux of phonons exchanging energy with each other and not just a free wave propagation. The possible mechanisms of energy redistribution between the phonons (pointed out in Ref. [2]) are phonon scattering on defects, nonlinear phonon-phonon interaction, or finite size effects. The interaction between the phonons might be due to the umklapp process [17].

We thank R. Quinn for useful discussions. S. N. acknowledges the Japan Society of the Promotion of Science.

*Present address: National Institute for Advanced Industrial Science and Technology, Tsukuba, Ibaraki 305-8561, Japan.

[1] H. Carslaw and J. Jaeger, *Conduction of Heat in Solids* (Clarendon, Oxford, 1959).
[2] B. Yang and G. Chen, Phys. Rev. B **67**, 195311 (2003).
[3] S. Lepri, R. Livi, and A. Politi, Phys. Rep. **377**, 1 (2003).
[4] B. Li and J. Wang, Phys. Rev. Lett. **91**, 044301 (2003).
[5] A. Dhar, Phys. Rev. Lett. **86**, 5882 (2001).
[6] S. Lepril *et al.*, Phys. Rev. Lett. **78**, 1896 (1997).
[7] M. Hoppenbrouwers and W. van de Water, Phys. Rev. Lett. **80**, 3871 (1998).
[8] H. Jaeger *et al.*, Rev. Mod. Phys. **68**, 1259 (1996).
[9] H. Thomas and G. Morfill, Nature (London) **379**, 806 (1996).
[10] D. Samsonov *et al.*, Phys. Rev. Lett. **83**, 3649 (1999).
[11] D. Samsonov *et al.*, Phys. Rev. Lett. **88**, 095004 (2002).
[12] S. Nunomura *et al.*, Phys. Rev. Lett. **89**, 035001 (2002).
[13] S. Zhdanov *et al.*, Phys. Rev. E **68**, 035401 (2003).
[14] D. Samsonov *et al.*, Phys. Rev. Lett. **92**, 255004 (2004).
[15] S. Nunomura *et al.*, Phys. Rev. E **65**, 066402 (2002).
[16] L. Landau and E. Lifshitz, *Fluid Mechanics* (Pergamon, New York, 1959).
[17] C. Kittel, *Introduction to Solid State Physics* (Wiley, New York, 1966), 3rd ed..